International Journal of Automotive Technology, Vol. 8, No. 4, pp. 403–411 (2007)

1229-9138/2007/035-02

ANALYSIS OF GAS-DYNAMIC EFFECTS IN COMPACT EXHAUST SYSTEMS OF SMALL TWO-STROKE ENGINES

J. GALINDO*, J. R. SERRANO, H. CLIMENT and A. TISEIRA

CMT Motores Térmicos, Universidad Politécnica de Valencia, Valencia 46022, Spain

(Received 18 July 2006; Revised 9 February 2007)

ABSTRACT–This article describes a methodology based on experiments and 1D modeling work related to the exhaust system analysis of a small two-stroke engine. The primary goal of this work was to understand how the design criteria of a compact exhaust system influenced the exhaust port pressure, since its evolution controls not only engine performance but also exhaust emissions. On the experimental side, a fully instrumented 50cc two-stroke engine was used to check the behavior of three different exhaust systems. A problem related to instantaneous pressure measurements in unsteady, hot flow was detected and solved during the study. To build the 1D model of the three exhaust systems, experimental information on the steady flow and the impulse test rigs was obtained under controlled conditions in specific facilities. Accurate comparisons between measured and calculated exhaust port instantaneous pressures were obtained from the following different exhaust system configurations: a straight duct, a tapered pipe and the three compact exhaust systems. The last step in the method used this model to analyze the pressure waves inside the exhaust system and detect the influence of the geometric parameters. The results should lead to improvements in the design process of complex compact exhaust systems in two-stroke engines.

KEY WORDS : Two-stroke engine, Exhaust system, Design, Modeling

1. INTRODUCTION

Within the forthcoming years, small, two-stroke engines, which are widely used in mopeds and scooters, will have to achieve strict anti-pollution standards. Different approaches are being explored for the future design of these engines. On the one hand, exhaust emissions reduction technologies have been investigated (Leighton *et al.*, 1994; Duret *et al.*, 1988; Nuti *et al.*, 1997; Payri *et al.*, 2001), and on the other hand, current engine systems with different technologies (carburettor, direct injection, catalyst) are being improved and evaluated in terms of emission control (Czerwinski *et al.*, 2006). In conjunction with this latter point of view, the development and application of tools to aid this engine design process should be studied.

It is a well-known fact (Blair, 1995) that the exhaust system design has a great influence on ported, crankcase-scavenged, small-capacity, two-stroke engines. This fact is observed not only in engine performance but also in noise and pollutant emissions. Computer modeling is a perfect tool to study the fluid dynamics occuring inside internal combustion engines. Wave action models, which solve the unsteady, non-linear and one-dimension flow equations, have been widely used to model exhaust systems. Obtaining the gas pressure evolution in the exhaust port is highly relevant, as it controls the scavenging process, i.e., burnt gases blowdown from the cylinder and fresh mixture trapping for the next engine cycle.

A huge amount of work has been carried out during the last few decades in relation to the typical expansion chamber pipe (Huessle, 1968; Blair and Johnston, 1970). This exhaust system consists of a divergent cone, a straight duct and a convergent cone, followed by another straight, long and narrow duct connected to a muffler. Today, however, exhaust systems are more compact and are referred to as having a multi-expansion chamber design in small spark-ignited two-stroke engines used in mopeds (Chiou *et al.*, 1994). This is comprised of a divergent cone that discharges to a chamber, followed by other chambers, which are connected in series using ducts. This paper provides a detailed analysis of the fluid dynamics inside this compact exhaust system design, including computer simulations compared with experimental information from the actual engine test bench.

2. METHODOLOGY

We believe engine testing in combination with accurate models is a key factor in achieving productive results.

**Corresponding author.* e-mail: galindo@mot.upv.es

Rather than focusing on the number of tests to be performed, it is essential to perform such tests with the highest possible accuracy. There are several advantages to comparing modeling and experimental strategies when solving a problem. On one hand, computer simulation costs are generally lower than those derived from experimental testing. Moreover, simulation results are obtained more quickly than in the testing, although this may not be true when 3D codes are used. On the other hand, specific facilities must be used to test a given system under controlled conditions in order to develop an accurate model. Furthermore, even if the absolute values of model predictions do not accurately reflect experimental data, they usually show correct trends.

Traditionally, wave propagation phenomena during gas exchange processes inside internal combustion engines are assumed to be one-dimensional. In the case under consideration, a wave action model, which solves the unsteady, non-linear and one-dimensional flow equations using a finite difference scheme (Payri *et al.*, 1991), was used to model a 50cc engine. Specific equations are implemented in the code to solve engine elements where the flow cannot be considered as one-dimensional, such as cylinder, crankcase, chambers, sudden area changes, and duct junctions. These boundary conditions are solved using the method of characteristics and then coupled with the finite difference calculation in the ducts (Payri *et al.*, 1996).

The governing equations that describe the one-dimensional non-homentropic gas flow, with the consideration of area change, friction and heat transfer in a pipe, form a non-homogenous hyperbolic system, and are represented in vector notation as follows (Daneshyar, 1976):

$$\frac{\partial \mathbf{W}}{\partial t}+\frac{\partial \mathbf{F}}{\partial x}+\mathbf{C}_1+\mathbf{C}_2=0 \tag{1}$$

This conservation law system, comprising the continuity, momentum and energy equations, is complemented by the equation of state or the real gas properties (Winterbone and Pearson, 1992). In equation 1, W is the desired state vector of the solution, F is the flux vector and C the source term separating the effect of the area changes from the effect of friction and heat transfer. The one-dimensional gas flow governing equations was traditionally arranged in the vector form shown in equation (2):

$$\mathbf{W}(x,t)=\begin{bmatrix}\rho\\ \rho u\\ \rho\left(\frac{u^2}{2}+\frac{p}{\gamma-1}\right)\end{bmatrix}\quad \mathbf{F}(\mathbf{X})=\begin{bmatrix}\rho u\\ \rho u^2+p\\ u\left(\frac{u^2}{2}+\frac{\gamma p}{\gamma-1}\right)\end{bmatrix} \tag{2}$$

$$\mathbf{C}_1(x,\mathbf{W})=\begin{bmatrix}\rho u\\ \rho u^2\\ u\left(\frac{u^2}{2}+\frac{\gamma p}{\gamma-1}\right)\end{bmatrix}\frac{1}{S}\frac{dS}{dx}\quad \mathbf{C}_2(\mathbf{W})=\begin{bmatrix}0\\ g\rho\\ -q\rho\end{bmatrix}$$

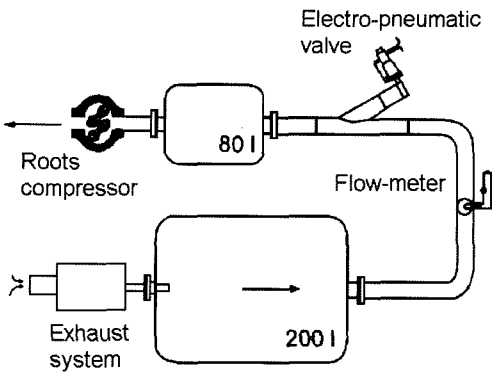

Figure 1. Steady flow test rig arrangement.

This set of equations is solved by using the two-step Lax-Wendroff method (Richtmayer and Morton, 1967), which is programmed in the computer code together with the boundary conditions.

As for the experimental tasks, three different facilities were used in this study, which led to the evaluation of the exhaust system design. First, a flow test rig and an impulse test rig provided the information required to set up the model for all the engine subsystems. The flow test rig gave the overall pressure loss in the element and the impulse test rig provided the reflection and transmission coefficients, which were required to develop the exhaust system model. Finally, an engine test rig was used to validate the model results.

In the flow test rig, a steady flow, which is supplied by means of a roots compressor, is forced to pass across the exhaust system. A scheme of the steady flow facility is provided in Figure 1. Variables such as air mass flow, and pressure and temperature at the exhaust system inlet and outlet, are measured.

The impulse test rig has been widely used in the dynamic characterization of exhaust elements in reciprocating engines using the impulse method (Payri *et al.*, 2000). The impulse test rig, whose schematic layout is

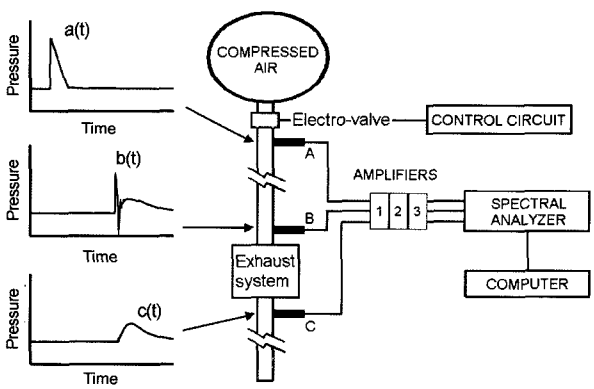

Figure 2. Impulse test rig arrangement.

shown in Figure 2, consists of a volume with compressed air, a fast-action valve and two long ducts. The exhaust system is placed between two ducts, which are long enough to avoid any wave overlap.

In the experiment, a fast valve operation produces a discharge of compressed air into the pipe. This compression wave travels towards the open end, passing through the exhaust system. The exhaust system behavior to this incident wave is perfectly determined since three instantaneous pressure measurement points with piezoelectric transducers are established in this test. The transducers are placed at the beginning of the discharging pipe (A), and at the inlet (B) and outlet (C) of the exhaust system.

The exhaust system tested in the two previous facilities was placed in a 50cc spark-ignited engine. This is a crankcase-scavenged type, single-cylinder two-stroke engine. The test bench, shown schematically in Figure 3, was fully instrumented to carry out performance and emissions measurements. Primary measurement devices consisted of an eddy-current electric brake up to 6 kW power, a hot wire anemometer to measure the air mass flow entering the engine, a gravimetric balance to register the fuel consumption and a Horiba Mexa 1300 exhaust gas analyzer to collect HC, NO and CO emissions. Firing tests were carried out at different load and engine speed conditions, since an electronic module controlled the brake as well as the throttle position. The engine had a liquid cooled cylinder, so a second cooling system was designed and built in order to control the engine coolant temperature.

Fluid flow properties are also relevant in checking the model accuracy. Mean temperatures and pressures were measured at the intake and exhaust pipes with thermocouples and manometers. Moreover, pressure transducers were placed in the cylinder, crankcase, and exhaust port in order to measure the instantaneous evolutions (every 0.5 crank angle degree).

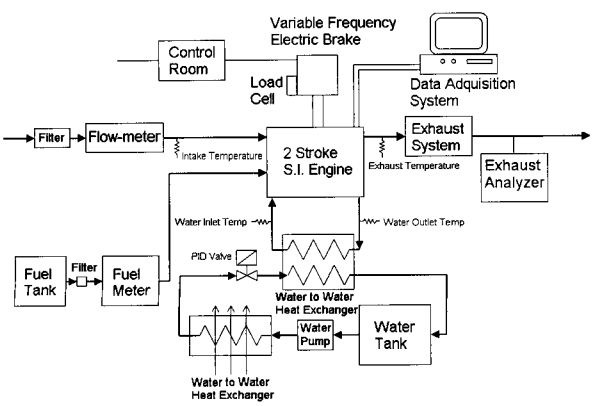

Figure 3. Schematic engine test bench layout.

3. MODEL SET UP

Since the main objective of this work was to analyze the fluid dynamics inside the exhaust system, three different units were considered to check the accuracy of the modeling methodology and to achieve a more representative study. All of them were based on the same configuration, which consisted of a divergent cone and several chambers placed in series joined by ducts. Schematic plots of these three different exhaust systems are shown in Figure 4.

The exhaust port is joined to the exhaust systems by a pipe, with a length of 240 mm and a diameter of 21 mm at the exhaust port and 25 mm in diameter at the exhaust system connection. Some relevant characteristics and differences among the exhaust systems are shown in Table 1.

All exhaust systems had the same inlet diameter (25 mm). ES#1 has the shortest cone length and the smallest cone angle, but the largest first chamber capacity. ES#2 and ES#3 have the same cone angle, which is 20% higher than in ES#1. ES#2 and ES#3 cone lengths are 27% and 42% higher than ES#1, respectively. ES#2 first chamber volume is 44% of ES#1, while ES#3 is 34%. The sizes of second and third chambers in all the exhaust systems

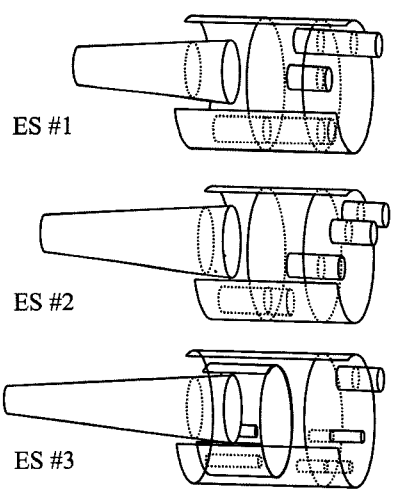

Figure 4. Schematic layout of the exhaust systems studied.

Table 1. Exhaust systems dimensions.

Exhaust system	#1	#2	#3
Inlet diameter pipe [mm]	25	25	25
Tapered pipe length [mm]	390	495	554
Tapered pipe angle [°]	4.25	5.1	5.1
First chamber capacity [cm^3]	2774	1220	943
Outlet diameter pipe [mm]	18	18	10 (x2)

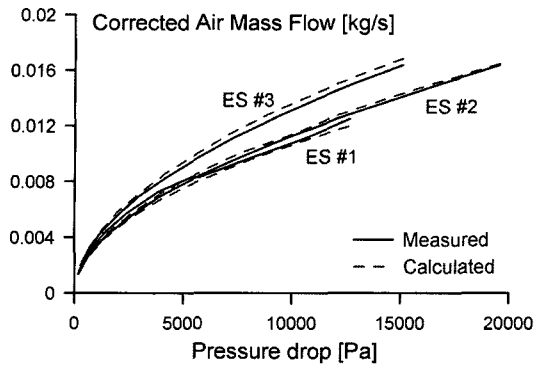

Figure 5. Flow test results.

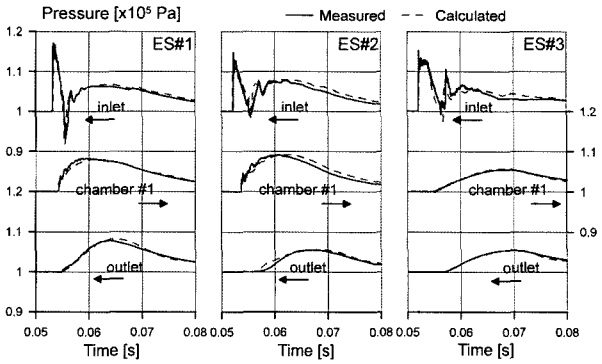

Figure 6. Impulse test results.

were 680 and 380 cm^3 respectively. The diameter of the pipes connecting the chambers in series is 18 mm, except for ES#3, where the diameter of the two ducts in parallel is 10 mm each. It was observed that as the cones size increased in size and divergence, the smaller the capacity of the first chamber. This is due to the fact that the overall volume is closely related to the time when the backward waves return to the cylinder. All of these exhaust systems are designed to allow the engine to achieve its optimum performance in the range of 7500 r/min.

Following this description of the various exhaust systems, the results of the modeling process can be presented. A discharge coefficient is required when a duct is connected to a chamber, since a 1D model cannot predict the flow effective area. The information obtained from the steady flow test rig is not sufficient to determine all the discharge coefficients in the exhaust system, since this test only provides the overall system pressure drop. For this reason, every discharge coefficient in the three exhaust systems was adjusted in order to reproduce the instantaneous pressure measured inside the various chambers in the impulse test experiment. At the end of this iterative process, the modeling results show good agreement when compared with both steady flow and impulse tests.

Results for the three exhaust systems in the flow test rig are shown in Figure 5, where the measured and modeled air mass flow is represented as a function of the pressure drop from the inlet to the outlet. ES#1 and ES#2 can be seen to show similar pressure loss characteristics. However, the overall pressure drop in ES#3 is lower than in the other two cases, due to the larger cross section of the two ducts connecting the chambers.

Instantaneous pressure traces predicted by the model when reproducing the impulse tests are plotted with experimental results in Figure 6. Additional measurement points were included in the classical test to check the model accuracy inside the exhaust system. Instantaneous pressure evolutions in the intermediate chambers were also registered. The inlet pressure experiences a sudden increase when the incident pulse arrives at the exhaust system. Soon after this, pressure decreases rapidly due to the expansion waves produced both in the divergent pipe and the first chamber discharge. Since the instantaneous mass flow entering the first chamber is higher than that exiting through the narrow pipe, a mass accumulation occurs in the first chamber, as observed in the instantaneous pressure plots. This causes a sudden increase in the inlet pressure, confirming the reflection of a compression wave. As the connecting pipe diameter between the first and second chambers is larger in ES#3, the emptying process is faster, as observed in the chamber#1 plot, with a lower peak and more rounded aspect. The instantaneous pressure at the exhaust system outlet shows slight compression and expansion processes depending on the entire exhaust system capacity. Since the whole size of ES#1 is the smallest, the outlet pressure presents a higher peak.

These results show a reasonably good agreement between calculated and experimental data. Since the models of the intermediate chambers do not take 3D phenomena into account, slight differences can be found in the chamber pressure evolution, mainly in ES#2. In relation to the pressure at the inlet of the exhaust system, the model proves to be able to predict not only the suction reflected wave appearing soon after the arrival of the incident pulse, but also the reflected compression peak in all cases. It is therefore possible to conclude that the models developed are perfectly valid for predicting fluid dynamics with an unsteady cold flow inside an exhaust system.

4. ENGINE RESULTS

4.1. Instantaneous Exhaust Pressure Measurement

To measure instantaneous pressure, both piezoresistive or piezoelectric transducers are widely applied. Both technologies were explored within this study with the aim of choosing the most convenient for this particular application. The piezoresistive transducer employed had the

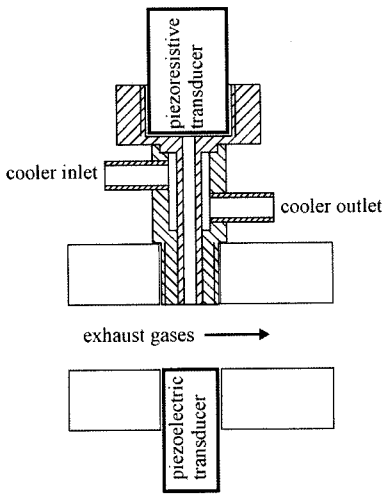

Figure 7. Schematic layout of a cooler used in piezoresistive transducers.

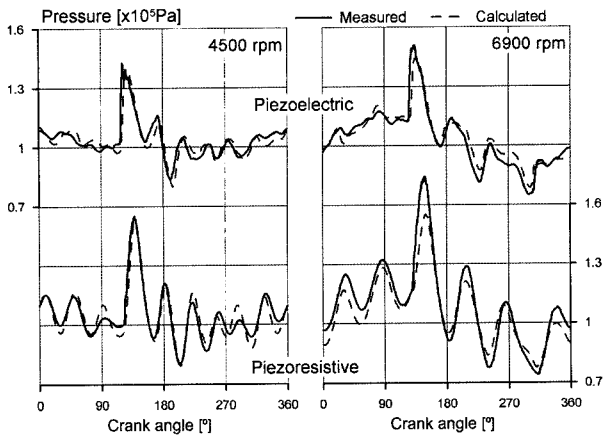

Figure 8. Measured and calculated exhaust port pressure with a duct exhaust system at full load.

advantage of measuring absolute pressure. However, in flows where temperature is very high, a special cooler (Figure 7) has to be placed between the duct and the sensor in order to reduce the temperature in the diaphragm and achieve repeatable measurements. When a piezoelectric transducer was used, there was no need to add a special cooler, so the device was placed directly at the pipe where the instantaneous pressure was measured. One disadvantage of employing this piezoelectric transducer was that the measurement is obtained in relative pressure, so the mean value was unknown.

The cooler geometry is by no means arbitrary. On one hand, it should be large enough to allow the inner flow to be cooled. It should be small enough to obtain instantaneous pressure as close to the pipe as possible. Despite the fact that the cooling duct diameter and length were chosen to be small, this cooler had a great impact on pressure measurements, as seen in the following data. Both measurement devices mentioned above were used simultaneously in order to compare the two instantaneous pressure signals. Thus, the piezoresistive (Kistler 4045A2) with the additional cooler and the piezoelectric (Kistler 6031) sensors were placed at the same cross-section in the pipe measurement point.

4.2. Constant Cross Section Pipe

Prior to viewing the results obtained by the simulations when modeling the exhaust system in real operating conditions, certain special engine tests were performed. First, the exhaust system was replaced by a long duct with a constant cross-section. The length and diameter of this duct were 550 mm and 25.5 mm, respectively. The primary goal was to check the accuracy of the results provided by the model with the easiest exhaust system to simulate. Then, within this context, model capabilities with non-steady and hot flow were evaluated.

The additional cooler geometry was determined and then modeled with the 1D code. Figure 8 shows the modeled and measured instantaneous pressures in the engine exhaust port as a function of the engine crank angle. Although an extensive number of tests were carried out, the results presented here correspond to an engine speed of 4500 and 6900 r/min, both at full load. The plotted results in the figure correspond to those registered with both the piezoelectric and piezoresistive transducers and significant differences can be seen between these signals. These differences in measurements are normally high frequency effects, caused by the standing wave in the short passage length of the cooling adapter. The natural frequency of the piezoresistive cooler is about 800 Hz, which corresponds to the natural frequency of a Helmholtz resonator with the cooler dimensions. This high frequency effect is easily removed in typical exhaust pressure measurements in four-stroke engines by using a low-pass filter. However, since a small two-stroke engine reaches very high rotating speeds and the engine performs one cycle per revolution, the frequency content of the pressure signals in the exhaust system is relevant even at frequencies higher than 800 Hz. The additional cooler influence is therefore quite significant.

Although the model is capable of simulating the additional cooler behavior and reproduce piezoresistive measurements, only the piezoelectric transducer is used to show instantaneous pressure measurements in the following figures. The mean pressure value is set equal to the mean value of the piezoresistive signal. The model can be seen to accurately predict the pressure pulses appearing inside the exhaust duct due to reflections in the atmosphere open end and in the cylinder exhaust port.

With regard to the model capabilities, two basic con-

clusions can be drawn from the close agreement of modeled and empirical data. The first conclusion refers to the interaction between the source, i.e. the cylinder, and the exhaust duct. The coupling of both models was correctly performed. The second conclusion is related to the heat transfer and exhaust temperature prediction in the duct, which is modeled accurately since wave propagation inside the duct is carried out in accordance with measured data.

The results provided by the model can now be used confidently to analyze the flow behavior inside this simple exhaust system configuration. In the wave action model, the forward pressure wave for a whole engine cycle, travelling from the cylinder to the exhaust system, is computed from the following (Payri *et al.*, 1995)

$$\left[\frac{p_f}{p_0}\right]^{\xi}=\frac{1}{2}+\left[\frac{p}{p_0}\right]^{\xi}\left(\frac{1}{2}+\gamma\xi\frac{u}{a}\right) \tag{3}$$

And the oppositely moving pressure wave

$$\left[\frac{p_b}{p_0}\right]^{\xi}=\frac{1}{2}\left[\frac{p}{p_0}\right]^{\xi}\left(\frac{1}{2}+\gamma\xi\frac{u}{a}\right) \tag{4}$$

In Figure 9, the modeled instantaneous pressure at different locations inside the duct is plotted on the top axis. These results are obtained at the exhaust port, at the middle and at the end of the duct (near the atmosphere open end). Models are therefore useful since they provide information that cannot be measured to analyze certain phenomena. The two lower plots below the same figure represent the forward and backward pressure waves appearing in the duct, calculated from equations (3) and (4), respectively. By following the space and time evolution of these pressure pulses, it is easy to understand the instantaneous pressure measured in the exhaust system.

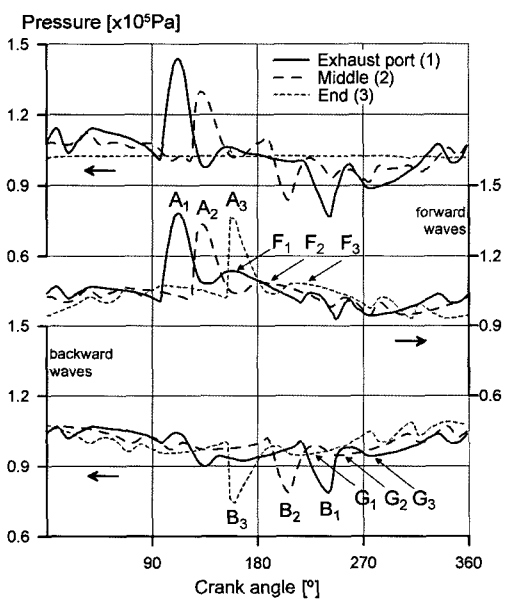

Figure 9. Calculated pressure waves with a duct exhaust system at full load and 5500 r/min.

The forward pulse, denoted as A_1, is due to the initial exhaust process as a consequence of the burnt gases discharged from the cylinder when the exhaust port opens. This pressure wave appears soon afterwards in the middle, A_2, and final, A_3, duct sections while travelling towards the atmosphere. The instantaneous pressure at the open end is approximately constant, so pulse A_3 is then reflected. The backward pulse, B_3, thus created begins to travel towards the cylinder, as waves B_2 and B_1 confirm. There is also another forward compression wave coming from the cylinder, F_1, leading to F_2 and F_3 at the consecutive analyzed points 2 and 3. This pressure wave is the consequence of the exhaust gases abandoning the cylinder when the transfer port opens and the crankcase content vents to the cylinder. The reflection of F_3 in the open end produces G_3, which travels back to the cylinder, resulting soon afterwards in G_2 and G_1. Pulses F and G can be easily followed in this particular exhaust system since the cross-section is constant. However, they are not as easily detected in the more complex cases shown in successive sections.

The distortion of both wave profiles A and B when moving forwards and backwards is evident. Since the value of propagation velocity is a function of the wave pressure and temperature at any point on the pressure wave, all the points on the wave propagate at different velocities and the wave shape changes in its passage along the constant cross-section duct. The superposition of forward and backward pulses make up the instantaneous pressure shown in the upper plot of the figure.

4.3. Tapered Pipe

The next step was to employ a divergent cone as an exhaust system to test model capabilities when simulating unsteady and hot flow inside tapered pipes. A comparison between measured and modeled results is shown in Figure 10 at engine full load and 4500 and 7500 r/min. As mentioned above, these measurements are only shown with the piezoelectric transducer. Predicted instantaneous pressure in the exhaust port presents quite a good agreement at both engine speeds. Therefore, it can be assumed that the wave action model also accurately calculates the fluid dynamics inside tapered pipes with an unsteady hot flow. It should be noted that the divergent cone angle was similar to those found inside previously detailed compact exhaust systems.

As previously performed with the constant cross-section duct, exhaust pressure wave analysis inside the tapered pipe can be seen in Figure 11. The cylinder blowdown when the exhaust port opens is related to pulse A, which moves toward the open end at atmospheric

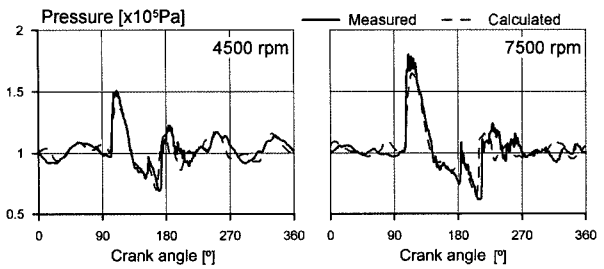

Figure 10. Measured and calculated exhaust port pressure with a tapered pipe exhaust system at full load.

conditions, resulting in peaks A_1, A_2 and A_3 at different tapered pipe locations. In this case, the wave amplitude diminishes as long as the pulse travels inside the pipe, due to the increase of the cross-section.

Since the model does not take into account any pressure loss at the open end, and the pressure is constant in the atmosphere, the reflection produces exactly the opposite wave to the incident pulse (A). This reflection creates a backward pressure wave with two clear characteristics: the expansion pulse B_3 and the compression pulse C_3. The propagation of the reflected pulse towards the cylinder, in particular B_3-C_3, is affected by the reduction of the cross-section and the distortion of the wave profile due to the different propagation velocities of the points on the wave. The consequences of these effects are the waves B_2-C_2 at the start of the cone and B_1-C_1 in the exhaust port.

The tapered pipe acts as an expansion to the area of the pipe system and sends continuous expansion wave reflections back. This explains the reduction in pulse A

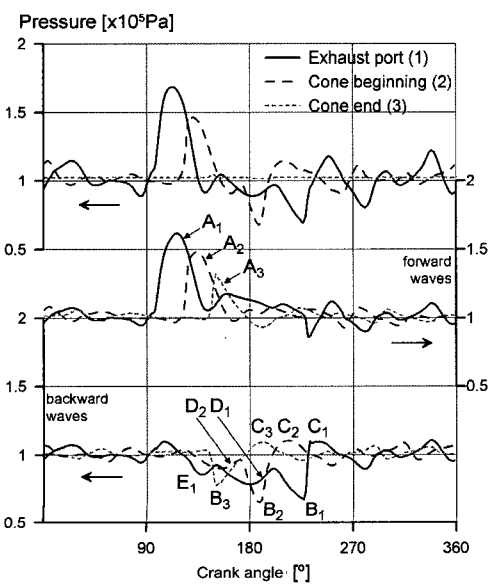

Figure 11. Calculated pressure waves with a tapered pipe exhaust system at full load and 8500 r/min.

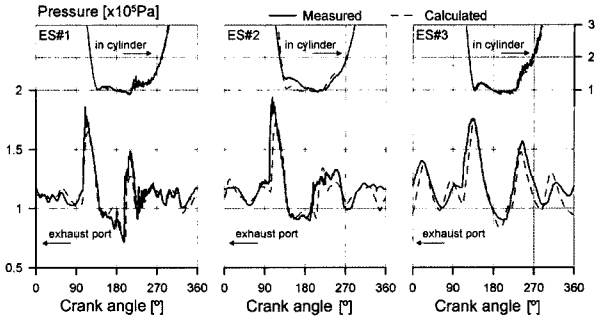

Figure 12. Measured and calculated exhaust port and in-cylinder pressure with different compact exhaust systems at full load and 7000 r/min.

amplitude and the creation of pressure wave D along the divergent cone, denoted in the plots as D_2 and D_1. It is obvious that this reflected wave is not registered in the final section of the cone, so D_3 does not appear in the figure. Finally, small reflections appear only in the exhaust port, named in figure E_1, depending on the duct geometry usually connecting the cylinder to the tapered pipe.

4.4. Compact Exhaust Systems

To conclude this section, the results obtained with the three different exhaust systems are compared with their corresponding data as measured in real firing engine conditions. Comparisons are presented in Figure 12. In this case, the instantaneous pressure in the engine exhaust port is shown as well as the pressure in the cylinder. While the exhaust port is open, i.e. between 90 and 270 crank angle degrees approximately, in-cylinder pressure also gives precise information on the scavenging process. These results correspond to 7000 r/min and full load engine conditions.

5. DISCUSSION OF THE RESULTS

This section analyzes the flow behavior inside the various exhaust systems. As in previous sections, the investigation of forward and backward moving pressure waves is very useful in understanding pressure evolution at the exhaust port. Therefore, instantaneous pressure at the exhaust port, at the beginning and at the end of the divergent cone are represented in the uppermost plots for all three exhaust systems in Figure 13. At these same points, the forward pulses are shown in the middle graph, and finally, the backward pressure waves can be observed in the lower plots. In all cases, the results are shown in the period where the exhaust port is open, since this is where significant information is shown.

As in previous sections, due to the exhaust port opening, pulse A appears and travels towards the open

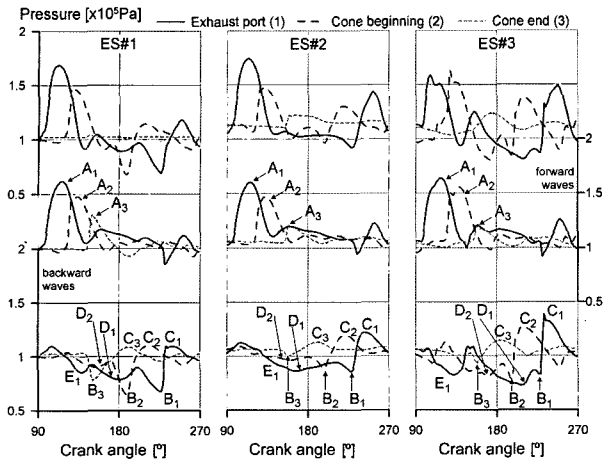

Figure 13. Calculated pressure waves with different compact exhaust systems at full load and 7000 r/min.

end. This pulse is denoted by A_2 and A_3 when it arrives at the beginning and end of the cone, respectively. The difference that can be highlighted among the three exhaust systems is in relation to the amplitude of this pulse when traveling through the cone. When the tapered pipe cone angle increases, the amplitude of the wave is reduced. This effect is observed in the lower peak of A_3 in ES#2 and #3 at the cone final section, contrary to that of ES#1.

The backward wave B_3 appears as a consequence of the reflection of pulse A_3 in the first chamber. The reflection in the case of a complete exhaust system cannot be performed in the same way as it was in the previous section with the duct or the tapered pipe. In fact, the reflection depends on the instantaneous pressure in the first chamber, closely related to its size and discharge capability to the second chamber through the narrow pipe. As mentioned above, the first chamber volume of ES#1 was very high, leading to an almost constant pressure inside, as depicted in the plot at the end of the cone (upper left of Figure 13). Thus, the larger the first chamber size, the higher the expected reflected pulse B_3. Therefore, the amplitude of the reflection B to the cylinder depends on both the magnitude of the incident wave, i.e. the tapered pipe cone angle, and the first chamber size.

Besides pulse B, the arrival of the incident pulse A to the first chamber also generates pressure wave C, which is a compression wave that goes back to the cylinder to retain the fresh mixture at the end of the scavenging process. The magnitude of pulse C_3 is again affected by the chamber size and the diameter of the exiting narrow pipe, that is, the filling and emptying behavior of the first chamber. If the chamber volume is small or the discharge to the second chamber is difficult, then the pulse C_3 compression peak increases. This effect is highlighted when the three different exhaust systems are compared, as shown in the figure. The propagation of pulse C to the cylinder is detected at the beginning of the cone (C_2) and at the exhaust port (C_1). The peak of this compression wave can be observed to increase due to the reduction of the cross-section in the cone when traveling back to the cylinder. In fact, this is clearly detected in ES#2 and #3, but not in #1 since the cone angle was the smallest.

As in the case of the tapered pipe, expansion waves other than those created in the first chamber appear in the exhaust system due to the reflection produced by pulse A along the cone, and these are detailed in the backward pressure figure as D_2 and D_1. The amplitude of this expansion wave depends on the cone angle and length. High values of these geometric characteristics give a more significant reflection as observed in the case of ES#3. Again, a backward wave E_1 could appear in the exhaust port due to the duct geometry connecting the cylinder with the exhaust system.

6. CONCLUSIONS

A methodology has been detailed to analyze the fluid dynamics inside compact exhaust systems. The main results can be summarized as follows:

(1) A methodology based on flow and impulse test rig experiments has been detailed to model three different exhaust systems. The tests are not difficult to perform and take into account both the steady and the unsteady flow behavior inside the system. They also provide precise information on pressure loss in compact exhaust systems made up of chambers connected in series.

(2) A step-by-step procedure has been established to confidently model a 50 cc two-stroke engine, including all the elements and placing special emphasis on the exhaust system. The work included the replacement of the exhaust system by: a) a constant cross-section duct, and b), a tapered pipe. The results provided by the model are in good agreement with the data measured on the engine test bench.

(3) Comparisons between simulation and experimental results are presented for the three different exhaust systems. In spite of the different flow behavior in each exhaust system, due to differences in design parameters, the model predicts the instantaneous pressures in the cylinder and in the exhaust port with acceptable accuracy.

(4) By using the simulation results it is possible to analyze the fluid dynamics inside an exhaust system. A detailed analysis based on the forward and backward pressure waves has been carried out to understand the influence of the exhaust design in the pressure profile at the exhaust port, which mainly

governs the scavenging process.

(5) In exhaust systems based on chambers connected in series, the pipe from the cylinder to the exhaust system, the divergent cone, the first chamber and the narrow pipe to the second chamber are the parameters to correctly design from the point of view of engine performance, i.e. not taking into account other criteria such as noise emission. If the capacity of the first chamber is high, a narrow but severe negative pressure pulse will be produced, which diminishes the compression reflected pulse. The extended, low amplitude wave that appears in the first stages of the scavenging process is influenced by the divergent cone geometry. High cone angles and long tapered pipes give a significant backward suction wave to the cylinder.

(6) The model shows accurate results when compared to measurements from the engine test bench at a wide range of operating points and with different exhaust system designs. However, we suggest a combination of modeling and experimental tasks to properly design compact exhaust systems in small two-stroke engines.

ACKNOWLEDGEMENT–The authors like to thank to the R+D+i Linguistic Assistance Office at the Universidad Politecnica of Valencia for their help in revising the paper.

REFERENCES

Blair, G. P. and Johnston, M. B. (1970). Simplified design criteria for expansion chambers for two-cycle gasoline engine. *SAE Paper No.* 700123.

Blair, G. P. (1995). Design and simulation of two-stroke engines. *R-161 Society of Automotive Engineers, Inc.*, Warrendale, PA.

Chiou, J. S., Chiang, M. S. and Chen, C. K. (1994). Numerical simulation method applied to the multi-expansion exhaust system of a two-stroke engine. *Proc. Instn. Mech. Engrs., Part D: J. Automobile Engineering,* **208**, 281-288.

Czerwinski, J., Compte, P., Reutimann, F. and Mayer, A. (2006). Influencing (nano)particle emissions of 2-stroke scooters. *Int. J. Automotive Technology* **7**, **3**, 237–244.

Daneshyar, H. (1976). *One-Dimensional Compressible Flow.* Pergamon Press. Oxford. New York.

Duret, P., Ecomard, A. and Audinet, M. (1988). A new two-stroke engine with compressed air assisted fuel injection system for high efficiency low emissions applications. *SAE Paper No.* 880176.

Huelsse, W. A. (1968). Investigation and tuning of the exhaust system of small 2-stroke-cycle engines. *SAE Paper No.* 680469.

Leighton, S. R., Cebis, M. J., Southern, M. P., Ahern, S. R. and Horner, L. (1994). The OCP small engine fuel injection system for future two-stroke marine engines. *SAE Paper No.* 941687.

Nuti, M., Pardini, R. and Caponi, D. (1997). Fast injection system: PIAGGIO solution for ULEV 2T SI engines. *SAE Paper No.* 970362.

Payri, F., Benajes, J. and Chust, M. D. (1991). Programme pour étude assistée par ordinateur de systèmes d'admission et d'échappement de moteurs. *Entropie,* **162**, 17–23.

Payri, F., Desantes, J. M. and Torregrosa, A. J. (1995). Acoustic boundary condition for unsteady one-dimensional flow calculations. *J. Sound and Vibration* **188**, **1**, 85–110.

Payri, F., Torregrosa, A. J. and Chust, M. D. (1996). Application of MacCormack schemes to I.C. engine exhaust noise prediction. *J. Sound and Vibration,* **195**, 757–773.

Payri, F., Desantes, J. M. and Broatch, A. (2000). Modified impulse method for the measurement of the frequency response of acoustic filters to weakly non-linear transient excitations. *J. Acoustical Society of America* **107**, **2**, 731–738.

Payri, F., Galindo, J., Climent, H., Pastor, J. M. and Gaia, C. (2001). Optimisation of the scavenging and injection processes of an air-assisted direct fuel injection 50cc 2-stroke S.I. engine by means of modelling. *SAE Paper No.* 2001-01-1814.

Richtmayer, R. D. and Morton, K. W. (1967). *Difference Methods for Initial-Value Problems.* Interscience. New York.

Winterbone, D. E. and Pearson R. J. (1992). A Solution of the Wave Equations Using Real Gases. *Int. J. Mechanical Sciences* **34**, **12**, 917–932.